

ATOMIC STRUCTURE AND MAGNETIC PROPERTIES OF COBALT DOPED ZnO THIN FILMS PREPARED BY THE SOL-GEL METHOD

J. NEAMTU, G. GEORGESCU, T. MALAERU, N.G. GHEORGHE^a,
R. M. COSTESCU^a, I. JITARU^b, J. FERRE^c, D. MACOVEI,
C. M. TEODORESCU*

*National Institute for Electrical Engineering, Splaiul Unirii 313, 074204
Bucharest, Romania*

*^aNational Institute of Materials Physics, Atomistilor 105b, P.O. box MG-7,
077125 Bucharest-Magurele, Romania*

*^b"Politehnica" University Bucharest, Spl. Independentei 313, 060042 Bucharest,
Romania*

*^cLaboratoire de Physique des Solides, UMR CNRS 8502, 91405 Orsay CEDEX,
France*

The ability of a sol-gel route for the synthesis of cobalt doped ZnO ($\text{Zn}_{1-x}\text{Co}_x\text{O}$, $x = 0.04-0.11$) films grown on Si (100) and glass substrates is investigated. A homogeneous and stable $\text{Zn}_{1-x}\text{Co}_x\text{O}$ sol was prepared by dissolving zinc nitrate hexahydrate and cobalt acetate tetrahydrate in a PVP (polyvinylpyrrolidone) solution, followed by annealing at 800 °C. Local structure studies of the $\text{Zn}_{1-x}\text{Co}_x\text{O}$ thin films by XANES (X-ray absorption near-edge structure) and EXAFS (extended X-ray absorption fine structure) proved the co-existence of a few amount of small metal cobalt aggregates with Co in non-stoichiometric Co_nO_m aggregates, with $n > m$, and $m \sim 4$. Low temperature magneto-optical Kerr effect (Faraday rotation) measurements of the magnetization versus field give a direct proof of a superparamagnetic behavior of the magnetic aggregates and allowed an estimate of the number of magnetically active atoms in Co aggregates, which is close to the number of Co excess atoms inferred from XANES and EXAFS considerations: $n - m \sim 3$ atoms per aggregate. To this main superparamagnetic phase, a weak ferromagnetic phase with coercitive field of ~ 50 Oe is superimposed, most probably due to metal cobalt nanoclusters.

(Received September 21, 2010; accepted after revision October 19, 2010)

Keywords: cobalt-doped ZnO; sol-gel growth; XAFS; magnetic properties

1. Introduction

Diluted magnetic semiconductors (DMS) are defined as structures with magnetic ions inserted into semiconductor lattices and where the ferromagnetic ordering can be induced by electrons and holes generated in the semiconductor [1,2], therefore providing carrier-mediated ferromagnetism by double exchange [2-4]. First studies dealt with insertion of manganese into GaAs or InAs [5], but these materials did not provide room temperature ferromagnetic ordering. Integrating manganese ions into other hosts (GaN, GaP, ZnSe, oxides: ZnO, TiO₂) emerged as an alternative to obtain room temperature ferromagnetism coupled with semiconductor properties of the material. Some years ago, Mn²⁺ ions incorporated into ZnO wurtzite structure was reported to exhibit this desired magnetic behaviour at room temperature [4]; it turned out rapidly that most of incomplete 3d shell metal ions can be used to produce ZnO-based DMS with room temperature ferromagnetism [4, 6-21]. However, the preparation conditions and levels of doping are crucial for the achievement of this goal. Of the 3d elements, Co is of special interest, since it provides a good

* Corresponding author: teodorescu@infim.ro

compromise between the ionic radius matching that of zinc (0.58 vs. 0.6 Å in tetrahedral coordination; 0.75 vs 0.74 Å in octahedral coordination, practically the same in other coordinations), allowing easy substitution of Zn in the ZnO wurtzite structure, together with considerable expected magnetic moment of 3 Bohr magnetons for the Co^{2+} ion. Indeed, $\text{Zn}_{1-x}\text{Co}_x\text{O}$ structures provided recently measurable ferromagnetism at room temperature [6,7].

However, the origin of this ferromagnetism was subject of a debate. First studies assessed an extrinsic origin of this ferromagnetism [8] connected to non-substitutional positions of Co ions in the ZnO lattice. Further studies evidenced the origin of ferromagnetism as being Co aggregates or clusters embedded in ZnO [9,10], whereas theoretical studies emphasized antiferromagnetic interaction between Co ions, which may be turned into ferromagnetic interaction by electron doping [11]. Subsequent structural and magnetic determinations revealed substitutional placement of Co ions into the ZnO lattice [7], with both ferromagnetic and antiferromagnetic coupling between Co ions. As free carrier sources which could mediate the ferromagnetic interaction there are acceptor-like states, which could be excess Co ions [12] or shallow donor-like states, typically oxygen vacancies or other growth imperfections [13-15]. However, the concentration of defects should not exceed a critical value, since this could yield to the annihilation of ferromagnetic ordering [16]. An alternative origin of ferromagnetic ordering from bound magnetic polarons, also generated by donor impurities was proposed [17]; also, controlled p-doping with Sn of zinc oxide - based DMS evidenced significant increase of both saturation magnetization and coercive field at room temperature [18]. Interstitial Zn atoms were also reported to contribute as donors to the room temperature ferromagnetism [19,20]. Subtle balances are nowadays taken into account involving charge compensation between n-doping originating from shallow donor states (oxygen defects) and p-doping coming from substitutional Co [14], antiferromagnetic coupling between Co ions coming close together at high doping levels [21], or antiferromagnetic coupling between magnetic ions induced by both oxygen vacancies and interstitial atoms [22].

The sol-gel method was successfully utilised in the past to synthesize room temperature Co-doped zinc oxide [7] and other ferromagnetic oxide-based DMS [10,13,14,20,21]. We adopted this technique since it is relatively cheap and provides control of the doping concentrations. As will be seen, the method did not provide diluted magnetic semiconductor properties, but instead the synthesis of very small cobalt oxide non-stoichiometric aggregates with a weak ferromagnetic phase superimposed. Nevertheless, interesting conclusions can be drawn from comparative structural and magnetic studies of these films.

Generally, the reported studies on transition metal doped oxides with magnetic properties: (i) determine the obtained structure by X-ray diffraction; the substitutional or non-substitutional placement of magnetic ions is derived from lattice parameters variations [7,10,13,14,20] (Vegard's law [23]); consequently, amorphous nanostructures or of aggregates with size beyond the X-ray diffraction limit (about 2 nm) cannot be detected; (ii) determine the local environment by IR [13], Raman [14], UV-visible [19], photo-luminescence [20] or X-ray photoelectron [7] spectroscopies; (iii) determine the magnetic properties, the magnetic susceptibility variation and sometimes the associated conduction properties. There are quite few X-ray absorption fine structure (XAFS) determinations. Particularly, Kittilstved et al. [19] have investigated both the pre-edge peak in the X-ray absorption near-edge structure (XANES) and the extended X-ray absorption fine structure (EXAFS) in cobalt doped ZnO prepared by chemical vapor deposition, with subsequent annealings in Zn vapor, followed by air oxidation. Striking similarities are reported between the Fourier transforms of the Co K-edge and the Zn K-edge EXAFS signals, while all statements about the pre-edge peak in XANES (generated by $1s \rightarrow 3d$ dipole forbidden transitions) rely on the similarity of the Co K-edge spectrum irrespective on the addition of Zn and subsequent annealing. No more quantitative analysis of the pre-edge peak was performed, as the main interest of the paper was to evidence reproducible behaviour of optical, conduction and magnetic properties upon zinc addition and oxidation, in order to emphasize charge carrier density control of ferromagnetism.

Consequently, the interplay between structure, composition and magnetism is crucial for these materials. In this paper we will report joint magnetometry (magneto-optical Kerr effect, MOKE) and local structure (XANES and EXAFS) studies of sol-gel synthesized ZnO:Co thin films, in order to emphasize the interplay between structure, stoichiometry, and magnetic

properties. The analysis of the pre-edge peak in XANES will be used in order to quantify the number of $3d$ vacancies per absorbing atom and thus to infer the Co ionization state [24]. EXAFS analysis will be used in order to derive the local atomic environment and the average aggregate size and composition. Magnetic measurements, which evidenced superparamagnetic behaviour even at very low temperatures (1.5 K), are used in order to derive the spin configuration of Co ions inside the cobalt oxide aggregates. The main question to be addressed by the structural studies presented here concerns the local atomic environment of cobalt into the ZnO wurtzite structure: (i) are Co metallic nanoclusters formed? (ii) is Co substituting Zn into the ZnO structure? (iii) are there some other local atomic arrangements formed, such as cobalt oxides, mixed cobalt and zinc oxides?

2. Experimental

$\text{Zn}_{1-x}\text{Co}_x\text{O}$ ($x = 0.2 - 0.3$) films were synthesized by using spin-coating method; the films were grown by sol-gel process either on Si (100) or glass substrates. Zinc nitrate hexahydrate $\text{Zn}(\text{NO}_3)_2 \cdot 6\text{H}_2\text{O}$ and cobalt acetate tetrahydrate $\text{Co}(\text{CH}_3\text{COO})_2 \cdot 4\text{H}_2\text{O}$ were used as precursors for preparation, and $(1 - x) \text{Zn}(\text{NO}_3)_2 - (x) \text{Co}(\text{CH}_3\text{COO})_2 - \text{PVP} - \text{H}_2\text{O}$ (where PVP are polyvinylpyrrolidone) as gelling agents. The cobalt concentration was 20, 25, 30 % of zinc nitrate, and the dopant salt was dissolved completely in PVP (polyvinylpyrrolidone). A mixture of $\text{Zn}(\text{NO}_3)_2$, $\text{Co}(\text{CH}_3\text{COO})_2$ and PVP in aqueous solution was refluxed 30 hours at 65 °C under continuous stirring. The substrates were cleaned using trichloroethylene, methanol and acetone before the film deposition.

The polycrystalline Co-doped ZnO thin films have been deposited from the above constituents by spin coating method (1500 RPM 30 seconds) on Si/SiO₂ and Crown glass substrates. This procedure was repeated four times. The pre-heated temperature for film stabilization after each layer deposition was 230 °C. The final films have been crystallized at 800 °C, during 1 – 4 hours. The estimated film thickness by using optical profilometry is 500 ± 75 nm.

Room and low temperature ZnO:Co (1.5 K) magneto-optical (MO) measurements were performed using green He-Ne laser light. At room temperature, the field dependence of the magnetization, $M(H)$ has been qualitatively deduced from Polar Faraday rotation (PFR) in transmission. Unfortunately, a too large MO contribution of the glass substrate, linear in H , avoids to make quantitative predictions on the $M(H)$ variation at room temperature. In order to determine the general $M(H)$ shape without ambiguity, we measured the magnetic circular dichroism (MCD) of the $\text{Zn}_{0.70}\text{Co}_{0.30}\text{O}$ film at low temperature (1.5 K) up to 2.4×10^6 A/m, to reach sample saturation.

X-ray absorption fine structure (XAFS: EXAFS and XANES) measurements were performed by using synchrotron radiation at the Doris storage ring facility in Hasylab, Hamburg, Germany. The XAFS spectra at the Co and Zn K-edges (7709 and 9659 eV, respectively) were recorded at the A1 beamline (EXAFS I experimental station), by using a Si(111) double crystal monochromator. The measurements were performed in fluorescence mode by using a 7-pixel SiLi detector and selecting the channels corresponding to the fluorescent radiation of interest (Co K_{α} , respectively Zn K_{α}). These measurements were performed on Co-doped ZnO obtained by spin coating. For consistent data interpretation, standards of metal Co and of Co(II)O were measured in the same experimental conditions; these latter experiments were performed in transmission mode on a 5 μm Co foil for the metal and of a pressed pellet of CoO powder mixed with cellulose. Special care was undertaken in order to keep the same monochromator calibration.

3. Results and discussions

Irrespective of preparation conditions, the XANES and EXAFS spectra of cobalt doped ZnO looked similar, both at the Co K-edge and at the Zn K-edge. This allowed the determination of Co concentration into ZnO, by comparison between the Co and Zn fluorescence signals reflected in the amplitude of the respective absorption edges. This concentration (atomic ratio

Co:Zn) ranges from $3.6 \pm 0.2 \%$ to $10.8 \pm 0.3 \%$. Therefore, a first result of this study would be that, in this concentration range, the local order about Co and Zn atoms is sensibly the same.

3.1. X-ray absorption near-edge structure spectroscopy

Figure 1 presents XANES spectra obtained at the Co K-edge on metal Co, on Co-doped ZnO, on Co(II)O, compared with the Zn K-edge spectrum of ZnO. The first remark is the striking similarity between the XANES of the Co (II) oxide and that of the Co in ZnO, with the exception of a small chemical shift of about 0.5 eV. Moreover, both Co K-edge XANES spectra exhibited the pre-edge peak, which is a sign of dipole forbidden transitions [19,24] $1s \rightarrow 3d$. Assuming that the integral amplitude of this peak is proportional to the number of $3d$ holes and the $4s^0 3d^7$ electronic configuration of Co^{2+} in CoO, one could infer the number of $3d$ vacancies as being $n_h(3d) = 2.0 \pm 0.1$ in ZnO:Co. From here, with a good approximation, a $3d^8$ configuration can be derived. The question is whether this configuration belongs to Co^+ ($4s^0 3d^8$) or to neutral Co atoms ($4s^1 3d^8$). The general aspect of XANES spectra and also the derived energy of the Co K edge suggest that the hypothesis of neutral Co can be ruled out, at least in what concerns the pre-edge peak: the XANES spectrum of metallic Co has completely different XANES resonances and also the pre-edge aspect is different. Consequently, hypothesis (i) formulated at the end of the Introduction section can be ruled out at this stage. This preliminary conclusion will be re-visited in a further paragraph, where all results (XANES, EXAFS and magneto-optical measurements) will be discussed altogether. Thus, one obtains the value of the ionization state of Co in the ZnO:Co samples, which is (in average) $+1.0 \pm 0.05$.

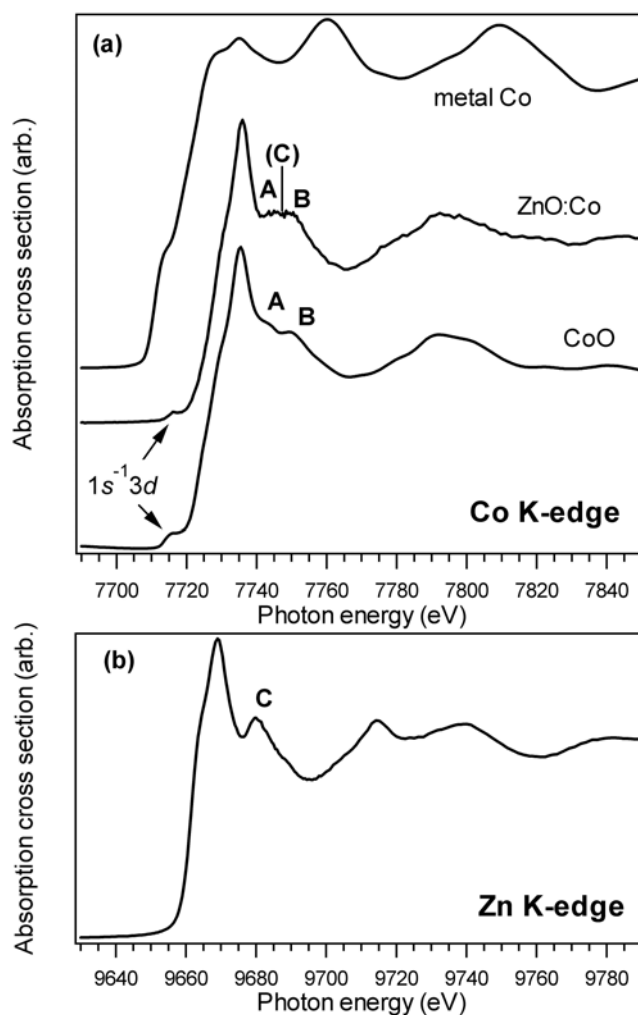


Fig. 1. (a) Co K-edge X-ray absorption near-edge structure (XANES) in metal Co, in ZnO:Co, and in Co(II) oxide, compared with (b) the Zn K-edge XANES spectrum in ZnO.

We remark here that the Zn K-edge spectrum [Fig. 1 (b)] is not similar to the Co K-edge XANES spectrum of Co-doped ZnO from Fig. 1 (a). In the Zn XANES spectrum, the pre-edge peak is missing, which is a sign of $4s^0 3d^{10}$ configuration of Zn^{2+} [19]. Also, the XANES spectrum is different. However, we cannot completely exclude some contribution of Co substituting Zn in the ZnO wurtzite lattice in the Co XANES of ZnO:Co, since it seems that after the white line in the Co spectrum there should be an additional contribution between what would be the next two XANES resonances if the spectrum were similar to that of CoO [denoted by A and B in Fig. 1 (a)]. This additional contribution could eventually originate from the first XANES resonance C after the white line in the Zn XANES spectrum [Fig. 1 (b)]. It seems then that most of Co atoms are placed in environments which are quite similar to that of cobalt (II) oxide, with eventually quite a few which substitute Zn in the ZnO structure. This preliminary statement will be discussed later in more detail.

3.2. Extended X-ray absorption fine structure spectroscopy

To gain more insight in the interplay between Co substituting Zn in ZnO and Co forming cobalt (II) oxide, we proceed with the analysis of the EXAFS data. The EXAFS function is defined as the relative variation of the absorption coefficient with respect to the atomiclike case $[\mu_0(k)]$: $\chi(k) = [\mu(k) - \mu_0(k)] / \mu_0(k)$. k is the photoelectron wave vector, $\hbar k^2 / (2m) = h\nu - E_0$, where E_0 is the energy of the absorption threshold and $h\nu$ is the photon energy ($\hbar = h/(2\pi)$ the Planck constant, m the electron mass). Figure 2 presents the k^3 -weighted EXAFS spectrum of the four situations discussed previously: Zn K-edge EXAFS in ZnO, Co K-edge EXAFS in ZnO:Co, Co K-edge EXAFS in Co(II)O and Co K-edge EXAFS in metal Co. Figure 3 presents the moduli of the Fourier transforms of the k^3 -weighted EXAFS function. The EXAFS data analysis followed the standard procedure discussed in Ref. [25]. Again, from Fig. 2 the presence of Co nanoclusters can be ruled out, since the EXAFS spectrum of metal particles should not deviate considerably from the EXAFS of bulk metal, which is quite different from the Co K-edge EXAFS of ZnO:Co. The EXAFS spectrum which is the most similar to that of Co in ZnO is again that of cobalt (II) oxide. This result is in line with the XANES observation.

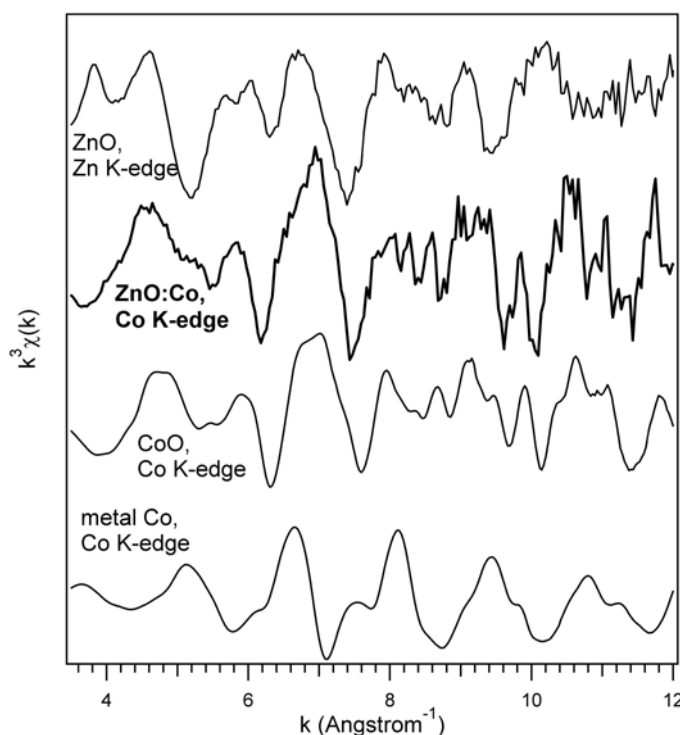


Fig. 2. k^3 -weighted extended X-ray absorption fine structure (EXAFS) spectra recorded at the Zn K-edge in ZnO, and at the Co K-edge in ZnO:Co, in Co(II) oxide and in metal Co.

More precise analysis can be done with the Fourier transforms (FT) of the EXAFS function (Fig. 3). Again, the Fourier transform of the EXAFS of Co metal is completely different. The Co EXAFS spectrum of Co in ZnO is close to the Co EXAFS spectrum in Co(II)O in the cubic rocksalt structure [26], at least in what concerns the first three coordination shells (with interatomic distances of 1.64, 2.58, and 3.13 Å). This is a first considerable difference from the EXAFS data presented in Ref. [19], where the FT of the Co K-edge EXAFS in ZnO:Co are similar to that of the Zn K-edge EXAFS in ZnO. The cobalt (II) oxide rocksalt (NaCl) structure presents around each Co atom a first coordination shell at distance $a/2 = 2.27$ Å [27] constituted by 6 oxygen atoms, followed by a second coordination shell at distance $a/2^{1/2} = 3.21$ Å with 12 Co atoms and a third shell at $3^{1/2}a/2 = 3.94$ Å with 8 oxygens. The difference of 0.6-0.8 Å with respect to the observed interatomic distances in the Fourier transform are due to the k dependence of phase shifts involved in the EXAFS function, namely the backscattering phase shift and the central atom phase shift [25].

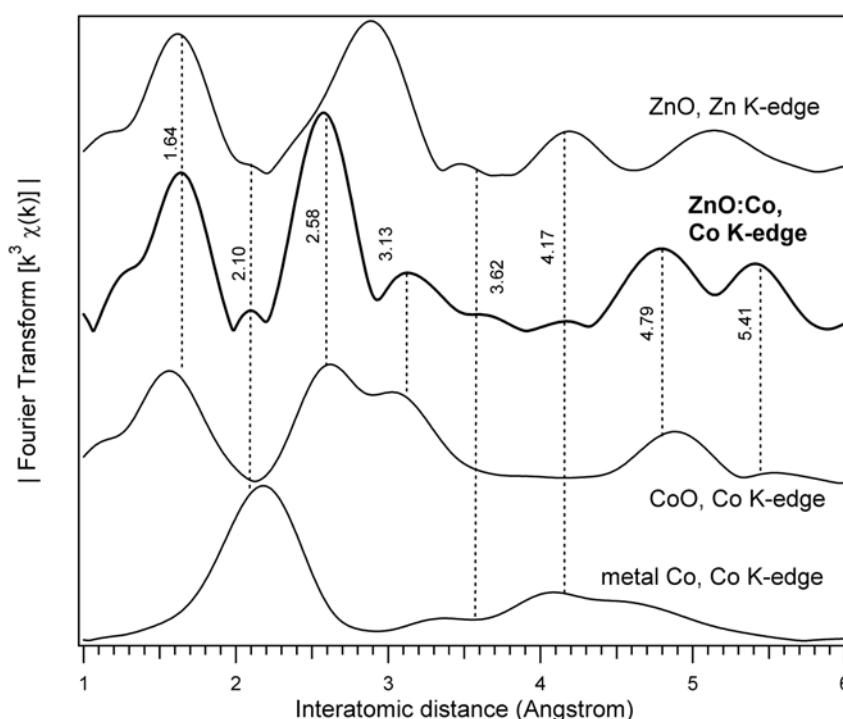


Fig. 3. Fourier transforms of the k^3 -weighted EXAFS functions recorded at the Zn K-edge in ZnO, and at the Co K-edge in ZnO:Co, in Co(II) oxide and in metal Co. Dashed lines are eyeguides.

However, the amplitudes of the FT peaks of the Co EXAFS in ZnO:Co are different from that of bulk Co(II)O. The main discrepancy is represented by the third coordination shell at 3.13 Å, whose amplitude is about 45 % of the amplitude of this peak in Co(II)O (related to the amplitude of the peak corresponding to the first coordination shell in FT). Also, the relative amplitude of the second coordination shell with respect to the first coordination shell increases.

The first explanation about this reduction of the number of atoms in the third coordination and the relative increase in the second coordination shell would be that Co ions are placed into small cuboidal aggregates of Co(II) oxide [28]. Some of the corresponding structures are represented in Fig. 4. Table 1 summarizes the computed average number of atoms in the first, second and third coordination shell ($\langle N_1 \rangle$, $\langle N_2 \rangle$, $\langle N_3 \rangle$) for some selected cobalt oxide aggregates: $\text{Co}_{13}\text{O}_{14}$ and $\text{Co}_{14}\text{O}_{13}$ spanning a cube with the edge a ; Co_4O_4 spanning a cube with the edge $a/2$, and two selected hypothetical non-stoichiometric clusters: (i) Co_7O_4 where three cobalt atoms have been added; (ii) Co_7O_3 where three cobalt atoms have been added and one oxygen was removed. Figure 4 presents also the hypothetical spin configuration of these aggregates, together with the computed numbers of first, second, and third order neighbors for all nonequivalent cobalt atoms.

The spin configuration of antiferromagnetic NiO was taken from Ref. [29]. The numbers of neighbors in Table 1 are obtained by averaging the coordination numbers from Fig. 4. Concerning the value of the ratio between the amplitudes of the Fourier transforms in the second (third) coordination shell and the first coordination shell, one may correct the "experimental" values from the last column in Table 1 by the experimental value obtained for bulk CoO (last-by-one column in Table 1). A relative increase of the number of second order neighbors by a factor of $1.37/1.05 = 1.30$ and a decrease of the number of third order neighbors with a factor $0.37/0.82 = 0.42$ may be derived. Multiplying with the theoretical values for CoO (first column), this implies that the structures measured have $\langle N_2 \rangle / \langle N_1 \rangle \approx 2.61$ and $\langle N_3 \rangle / \langle N_1 \rangle \approx 0.60$. The aggregate which presents the closest values of these ratios with the above derived values is Co_7O_3 .

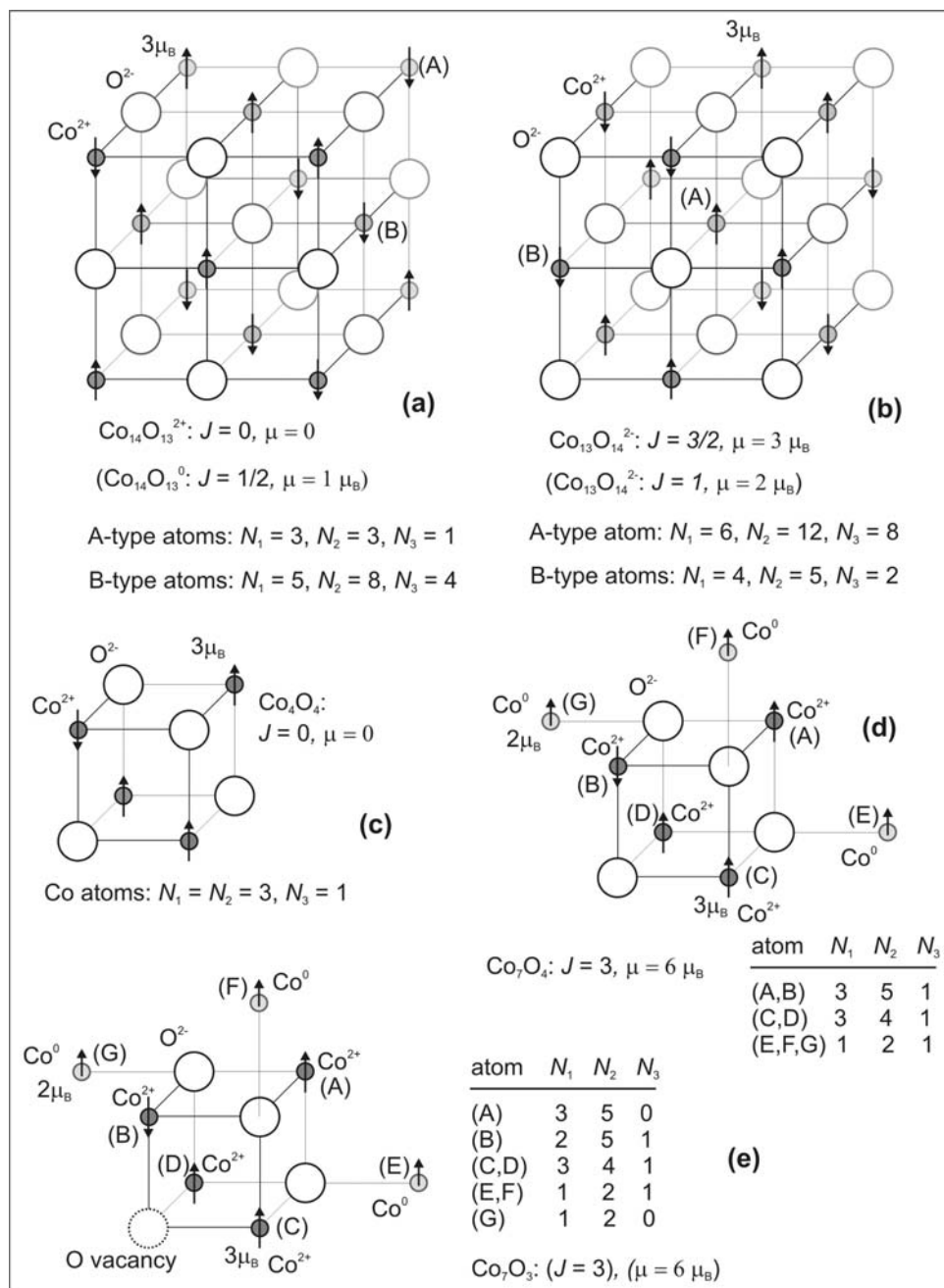


Fig. 4. Atomic and proposed spin configurations for (a) $\text{Co}_{14}\text{O}_{13}$; (b) $\text{Co}_{13}\text{O}_{14}$; (c) Co_4O_4 ; (d) Co_7O_4 ; (e) Co_7O_3 . The number of first, second and third shell neighbors (N_1 , N_2 , N_3) are also presented for each kind of non-equivalent Co atom.

Table 1. Average number of neighbors in the first three coordination shells around a cobalt atom, for selected cobalt oxide aggregates in rocksalt structure.

| Aggregate <N _j > | bulk Co(II)O | Co ₁₃ O ₁₄ | Co ₁₄ O ₁₃ | Co ₄ O ₄ | Co ₇ O ₄ | Co ₇ O ₃ | Exp. FT bulk | Exp. ZnO:Co |
|-------------------------------------|-----------------|----------------------------------|----------------------------------|--------------------------------|--------------------------------|--------------------------------|--------------------|----------------|
| <N ₁ > | 6 (O) | 4.15 | 3.86 | 3.00 | 2.14 | 1.71 | | |
| <N ₂ > | 12 (Co) | 5.54 | 5.14 | 3.00 | 4.28 | 4.28 | | |
| <N ₃ > | 8 (O) | 2.46 | 2.29 | 1.00 | 1.00 | 0.57 | | |
| <N ₂ >/<N ₁ > | 2.0 | 1.33 | 1.33 | 1.00 | 2.00 | 2.50 | 1.05 | 1.37 |
| <N ₃ >/<N ₁ > | 1.33 | 0.59 | 0.59 | 0.33 | 0.47 | 0.33 | 0.82 | 0.37 |

Such non-stoichiometric aggregates were indeed proven to exist by mass spectrometry. For instance, in Fig. 1 from Ref. [30], Co₇O₄ was visible in the mass spectrum. The same paper analyses also theoretically the stability of free cuboidal clusters, by focusing on Co₄O₄ and deriving that the ferromagnetic arrangement was the most probable one. This assumption is contrary to the spin configuration attributed in Fig. 4 above, but: (i) on one hand, the simulations from Ref. [30] yielded only a 200 meV energy difference between the ferromagnetic and the antiferromagnetic state; (ii) it might be possible that the interaction with the surrounding ZnO environment yields to the stabilisation of the antiferromagnetic configuration. Otherwise, as will be seen in the following, a stronger superparamagnetism should be exhibited by these clusters.

With larger interatomic distances, one could remark the occurrence of two peaks in the FT (at 3.62 and 4.17 Å) which are close to FT peaks of both the Zn EXAFS spectrum in ZnO, but also to the FT peaks in metal Co. If some cobalt is organized in Co nanoclusters, it may account for the occurrence of the small peak at 2.10 Å in the FT of the Co EXAFS of ZnO:Co, but this is in disagreement with the XANES observations. So, actually one cannot definitively state between co-existence of Co metal clusters + non-stoichiometric Co(II) oxide aggregates with excess Co, or between co-existence of non-stoichiometric CoO aggregates with Co substituting Zn in ZnO wurtzite lattice. After the analysis of the magnetic properties, we shall discuss again this point.

Nevertheless, the peak at 4.17 Å can be taken into account in order to evaluate the order of magnitude of the proportion of Co atoms in other environments than in CoO-like aggregates, since there is no structure in the Fourier transform of the Co EXAFS spectrum in Co(II)O in this region. From the estimate of the ratio between the integral amplitude of the peak at 4.17 Å between the Zn EXAFS spectrum and the Co EXAFS spectrum in ZnO:Co (weighted by the overall amplitude of the whole Fourier transform) one obtains that a maximum amount of 13.4 ± 3.7 % of the Co atoms could be in an environment similar to the Zn atoms in ZnO. A quite similar value of 13.0 ± 2.6 % is obtained when comparing with the FT of the metal Co EXAFS spectrum. We may note here that a similar factor of ~ 0.13 , when multiplying the sole C structure in the Zn XANES spectrum [Fig. 1(b)] could yield the structureless plateau observed in the Co XANES spectrum of ZnO:Co [Fig. 1(a)], between the XANES A and B structures belonging to the Co XANES spectrum of Co(II)O. But, similarly, the structure between the A and B XANES resonances can be smeared out by the addition of a small contribution proportional to the metal Co XANES spectrum, if one admits also the possibility of a shift of some ~ 12 eV, by aligning the absorption edges.

To conclude this paragraph of EXAFS analysis, the most plausible explanation is that the largest amount (≈ 87 %) of cobalt forms non-stoichiometric cobalt (II) oxide aggregates with stoichiometries close to Co₇O₃, with a smaller amount (~ 13 %) which may form either cobalt nanoclusters, either substituting zinc in ZnO wurtzite structure.

3.3. Magneto-optical Kerr effect measurements

Figure 5 presents MCD- magneto-optical Kerr effect (MOKE) measurements obtained at low temperature (1.5 K) on the film with Co atomic concentration of 11 %. The raw experimental data [insert (i.1) in Fig. 5] suggest the coexistence of the superparamagnetic phase with a weak ferromagnetic phase with coercitive field of about 50 Oersted. The experimental data were fitted a constant times the Brillouin function:

$$B_J \left(\frac{g\mu_B\mu_0 JH}{k_B T} \right) = \frac{2J}{2J+1} \cot \left(\frac{2J}{2J+1} \frac{g\mu_B\mu_0 JH}{k_B T} \right) - \frac{1}{2J+1} \cot \left(\frac{g\mu_B\mu_0 JH}{(2J+1)k_B T} \right) \quad (1)$$

in order to derive the value of the total moments participating to the paramagnetism J . For values of J exceeding the individual atomic moments, we may speak about superparamagnetism. In the above formula, g is the gyromagnetic factor of the electron (≈ 2), μ_B the Bohr magneton, μ_0 the vacuum permittivity and $k_B T$ the Boltzmann factor. The net result of the fit was $J = 3.0 \pm 0.1$, while the resulting temperature was 1.53 ± 0.7 K. Good quality fits were obtained also with smaller values of J , but the resulting temperature was unphysical (below 1 K). Setting values of J larger than 3 in the Brillouin formula visibly degrades the fit. Consequently, it may be inferred that the magnetic properties of these samples are governed by small nanoparticles with moments of about 6 Bohr magnetons, i.e. with three magnetically active metal-like Co atoms ($3d^8$) or two active Co^{2+} ions ($3d^8$).

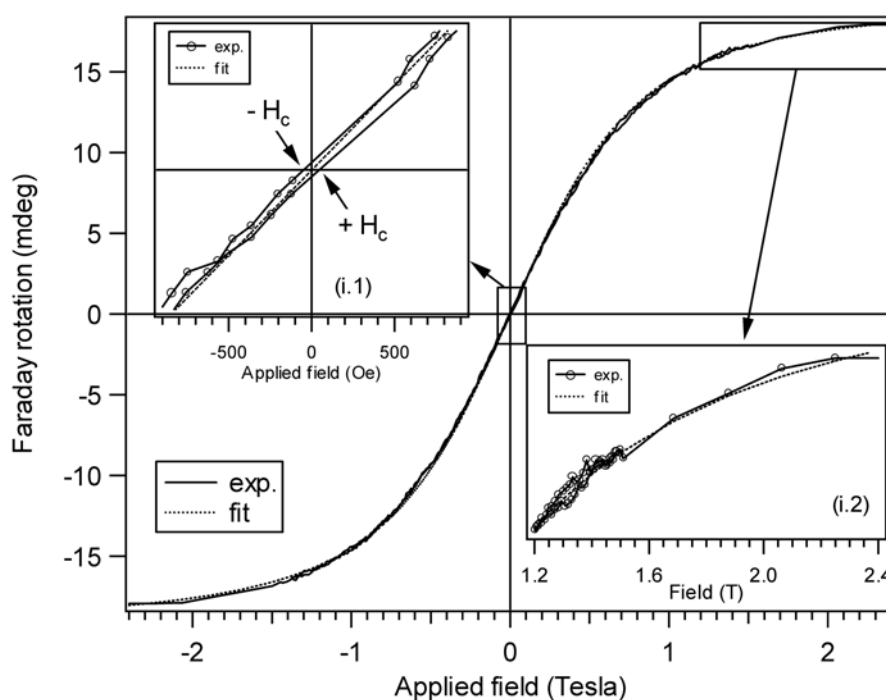


Fig. 5. Magnetic circular dichroism obtained at 1.5 K on the film with 11 % Co, together with a fit with a Brillouin function [eq. (1)] for $J = 3$ and $T = 1.53$ K. Inserts: (i.1) the region of weak fields, exhibiting the small coercitivity discussed in the text; (i.2) the region of elevated fields, in order to emphasize the quality of the fit.

By subtracting the fit with the Brillouin function from the raw experimental data, one may estimate that the "residual" ferromagnetic phase accounts for about 3 % of the observed magnetic signal.

3.4. Discussions

From the XANES data of the pre-edge region, it is inferred an average ionization state of +1.0 per Co atom. From the EXAFS analysis, ~ 87 % of the cobalt atoms are forming cobalt (II) oxide non-stoichiometric aggregates, the remaining ~ 13 % being either neutral, either Co^{2+} substituting Zn. We shall analyze the charge state of cobalt inside cobalt oxide aggregates ($q+$) in the two cases:

(a) 87 ± 4 % $\text{Co}_n^{q+}\text{O}_m^{2-}$ clusters with 13 ∓ 4 % neutral Co: $0.87 q + 0.13 \times 0 = +1$ yields $q = 1.15 \pm 0.05$. From the neutrality of cobalt aggregates, the ratio $m/n = 2/q \approx 1.74$, so the suggested basic

aggregate would be Co_7O_4 , ($n = 7$ and $m = 4$). This is close to the conclusion of the EXAFS analysis, where the most probable proposed structure was Co_7O_3 .

(b) $87 \pm 4\%$ $\text{Co}_n^{\text{qt}}\text{O}_m^{2-}$ clusters with $13 \mp 4\%$ substitutional Co^{2+} : $0.87q + 0.13 \times 2 = +1$ yields $q = 0.85 \pm 0.09$. In this case, $m/n = 2/q \approx 2.35$; the closest aggregate satisfying this is Co_7O_3 ($n/m = 7/3 = 2.33$).

We may also note that from the spin configurations proposed in Fig. 4, one may exclude the formation of larger aggregates, such as $\text{Co}_{13}\text{O}_{14}$ or $\text{Co}_{14}\text{O}_{13}$ (or bigger), since their overall magnetic moment of these aggregates is too low, owing to the antiferromagnetic character of bulk CoO. Alternatively, one may propose non-stoichiometric aggregates based on the above two cuboids, such as $\text{Co}_{25}\text{O}_{14}$, $\text{Co}_{23}\text{O}_{13}$, etc., but in this case one cannot unambiguously assign the spin configuration of the $n - m = 9-10$ atoms such as to construct the overall spin of 3 Planck units for such aggregates.

We have now to state which of the proposed situations is the most probable (Co_7O_4 aggregates together with neutral cobalt, or Co_7O_3 aggregates together with Co^{2+} substituting zinc), by taking into account all the observations discussed so far. Table 2 summarizes the findings of the employed techniques.

Table 2. Summary of the XANES, EXAFS and MO findings, as arguments for one of the two discussed situations

| Situation Technique | (~ 87 %) Co_7O_3 + (~ 13 %) Co^{2+} substitutional in ZnO | (~ 87 %) Co_7O_4 + (~ 13 %) metal Co clusters |
|---|---|---|
| XANES | <i>in favour</i> : Resonance C between A and B | <i>against</i> : no XANES features of metal Co |
| EXAFS | <i>in favour</i> : best fit to ratio $\langle N_2 \rangle / \langle N_1 \rangle$: 2.61 to be compared with 2.50 | <i>in favour</i> : best fit to ratio $\langle N_3 \rangle / \langle N_1 \rangle$: 0.60 to be compared with 0.47 |
| EXAFS | <i>against</i> : comparison of $\langle N_3 \rangle / \langle N_1 \rangle$: 0.60 to be compared with 0.33 | <i>against</i> : comparison of $\langle N_2 \rangle / \langle N_1 \rangle$: 2.61 to be compared with 2.0 |
| EXAFS | <i>against</i> : no visible peak corresponding to the second coordination shell in the EXAFS at the Zn K-edge | <i>in favour</i> : visible peak in the FT at 2.10 Å, similar to the first order peak in the FT of metal Co. |
| magnetometry $J = 3$ | <i>against</i> : impossible to configure a total $J = 3$ from three $3d^7$ ions with $J = 3/2$ and four $3d^8$ atoms with $J = 1$. | <i>in favour</i> : the three excess Co atoms are almost neutral with $3d^8$ configuration and their spins are alligned ($J = 1$ each). |
| magnetometry: ferromagnetic component | <i>against</i> : the residual ferromagnetic component is too weak to represent Co ions diluted in ZnO | <i>in favour</i> : the neutral Co atoms may not be ferromagnetic alligned in totality |

We agree that the discussion is somewhat very simplifying: most probably, both situations are encountered, together with a wide variety of other situations (larger aggregates, wide range of stoichiometries, etc.). Also, it is clear that the exact geometries of Co_7O_4 and Co_7O_3 are not that of Fig. 4. Instead, we used these simplified pictures in order to explain roughly the modification of number of neighbors and the spin states of these clusters. Molecular dynamics calculations are needed to get more insight in the electronic structure and geometry of these aggregates, but this is beyond the scope of our paper. We just would like to state which is the most probable situation. Taken together, the arguments presented in Table 2 suggest that the most probable situation is (~ 87 %) Co_7O_4 + (~ 13 %) metal Co clusters. The argument of too elevated experimental value of $\langle N_2 \rangle / \langle N_1 \rangle$ can be counteracted by observing that the theoretically computed values were for isolated aggregates and, in reality, the effective number of neighbours should include the atoms from the matrix, which could give significant contribution in the second and third coordination shell. Also, the XANES spectra of metal-like cobalt could be smeared out into the overall superposed XANES spectrum, since the metal XANES spectrum is much less structured. The XANES structures A and B from bulk CoO may also be smeared out owing to the size and non-stoichiometry effects of the small aggregates, as it was demonstrated for non-stoichiometric Na_nF_m

($n > m$) aggregates in Ref. [28]. We conclude by proposing that, most probably, the investigated samples present co-existence of cobalt metal nanoparticles with small aggregates quite close in stoichiometry with Co_2O , with almost monovalent cobalt, and no cobalt substituting zinc in the ZnO structure.

At the same time, the "residual" ferromagnetic phase which represents roughly 3 % from the total moment of the unit volume, can be attributed rather to the formation of neutral Co nanoclusters which are only partly ferromagnetic ordered in the crystal than to the Co^{2+} ions substituting Zn and participating to this weak ferromagnetism. An estimate of the magnetic moment per cobalt atom in this ferromagnetic phase follows: the major phase is formed by non-stoichiometric clusters with average magnetic moment $6/7 \approx 0.86$ Bohr magnetons per atom. The residual phase represents $0.13/0.87 \approx 15$ % from the major phase (in terms of cobalt atoms) and has about 3 % of the total magnetic moment. Therefore, the magnetic moment per cobalt atom in the ferromagnetic phase would be $0.03 \times 0.86 / 0.15 \approx 0.17$ Bohr magnetons. If we attribute the theoretical value of 2 Bohr magnetons to a neutral cobalt atom, it follows that one has a $2\mu_B$ ferromagnetic aligned cobalt for $2/0.17 \approx 12$ cobalt atoms which do not contribute to the magnetism. In a cluster shell model, a small Co aggregate could be imagined as an icosahedral, *fcc* or *hcp* packing unit of 13 cobalt atoms, where only the central atom participates to the ferromagnetic order, the others being "magnetically dead", being situated at the interface with the matrix. Such simple picture cannot be drawn, if one attributes that the formation of the weak ferromagnetic order comes from Co^{2+} placed in substitutional sites.

The diluted magnetic semiconductor character of the structures synthesized in this work is therefore questionable; nevertheless, the derived spin state (with the excess Co atoms having parallel spins) could be of interest for the investigation of similar moieties quite similar in electronic structure, such as iron-sulfur aggregates (Fe_4S_4 , Fe_7S_4 , Fe_7S_3 , etc.), which are intensively studied in biochemistry [31] during the last years owing to their prime importance in photosynthesis, catalysis, enzymology, molecular electronics etc. Small non-stoichiometric cobalt oxide clusters with net spin moment could also find other applications in magnetic field sensing. Also, an eventual magnetic long range order may be induced between these aggregates by varying the carrier density by external doping [18,19]. Also, there are quite new applications of cobalt oxide nanoclusters in the field of catalysis [32] and especially as carbon-free molecular water oxidation catalysts, based on Co_4O_4 cores [33].

4. Conclusion

At present, the sol-gel route chosen seems to be inappropriate to synthesize Co-doped ZnO materials with diluted magnetic semiconductor behaviour. Nevertheless, the fact that a weak ferromagnetic phase was observed at very low temperature (1.5 K) is encouraging.

Instead, the proposed method seems to be appropriate to synthesize materials where very small Co_nO_m non-stoichiometric aggregates (a few atoms, most probable stoichiometry Co_7O_4) are formed, coexisting with structures where Co is in a chemical state and atomic environment very close to Co metal. It is also inferred that these metal nanoclusters are not very large, being estimated at few more than ten Co atoms. The utility of the present study stems in being amongst the first studies to combine (i) magnetometry, including fitting of the superparamagnetic behaviour with: (ii) pre-edge structures in XAFS giving insight about the ionization state and the number of $3d$ vacancies; (iii) analysis of XANES resonances; (iv) analysis of EXAFS spectra. The joint analysis of magnetism and X-ray absorption spectroscopic data yielded a consistent picture about the intimate structure of the synthesized materials.

Acknowledgements

This work was supported by the Romanian National Authority of Scientific Research under the contract CNCSIS PCCE ID_76/2010. We gratefully acknowledge support from Dr. D. Zajac and Dr. E. Welter from the Hasylab staff.

References

- [1] H. Munekata, H. Ohno, S. Von Molnár, A. Segmuller, L.L. Chang, and L. Esaki, *Phys. Rev. Lett.* **63**, 1849 (1989); H. Ohno, *Science* **281**, 951 (1998); H. Ohno, D. Chiba, F. Matsukura, T. Omiya, E. Abe, T. Dietl, Y. Ohno, and K. Ohtani, *Nature* **408**, 944 (2000); M. Yamanouchi, D. Chiba, F. Matsukura, and H. Ohno, *Nature* **428**, 539 (2004).
- [2] T. Dietl, H. Ohno, F. Matsukura, J. Cibert, and D. Ferrand, *Science* **287**, 1019 (2000).
- [3] H. Munekata, T. Abe, S. Koshihara, A. Oiwa, M. Hirasawa, S. Katsumoto, Y. Iye, C. Urano, and H. Takagi, *J. Appl. Phys.* **81**, 4862 (1997); H. Akai, *Phys. Rev. Lett.* **81**, 3002 (1998); S. Das Sarma, E.H. Hwang, and A. Kaminski, *Phys. Rev. B* **67**, 155201 (2003).
- [4] K. Ueda, H. Tabata and T. Kawai, *Appl. Phys. Lett.* **79**, 988 (2001); S.J. Pearton, C.R. Abernathy, M.E. Overberg, G.T. Thaler, D.P. Norton, N. Theodoropolou, A.F. Hebard, Y.D. Park, F. Ren, J. Kim, L.A. Boatner, *J. Appl. Phys.* **93**, 1 (2003); M. Venkatesan, C.B. Fitzgerald, J.G. Lunney, and J.M.D. Coey, *Phys. Rev. Lett.* **93**, 177206 (2004).
- [5] H. Ohno, H. Munekata, S. Von Molnár, and L.L. Chang *J. Appl. Phys.* **69**, 6103 (1991); H. Ohno, H. Munekata, T. Penney, S. Von Molnár, and L.L. Chang, *Phys. Rev. Lett.* **68**, 2664 (1992); H. Ohno, A. Shen, F. Matsukura, A. Oiwa, A. Endo, S. Katsumoto, and Y. Iye, *Appl. Phys. Lett.* **69**, 363 (1996); B. Beschoten, P.A. Crowell, I. Malajovich, D.D. Awschalom, F. Matsukura, A. Shen, and H. Ohno, *Phys. Rev. Lett.* **83**, 3073 (1999); C.M. Teodorescu, M.C. Richter and K. Hricovini, *J. Optoe. Adv. Mater.* **8**, 1200 (2006).
- [6] K. Ueda, H. Tabata, and T. Kawai, *Appl. Phys. Lett.* **79**, 988 (2001); M. Kobayashi, Y. Ishida, J.I. Hwang, T. Mizokawa, A. Fujimori, K. Mamiya, J. Okamoto, Y. Takeda, T. Okane, Y. Saitoh, Y. Muramatsu, A. Tanaka, H. Saeki, H. Tabata, and T. Kawai, *Phys. Rev. B* **72**, 201201 (2005).
- [7] H.J. Lee, S.Y. Jeong, C.R. Cho, and C.H. Park, *Appl. Phys. Lett.* **81**, 4020 (2002).
- [8] S.C. Wi, J.S. Kang, J.H. Kim, S.B. Cho, B.J. Kim, S. Yoon, B.J. Suh, S.W. Han, K.H. Kim, K.J. Kim, H.J. Song, H.J. Shin, J.H. Shim, and B.I. Min, *Appl. Phys. Lett.* **84**, 4233 (2004).
- [9] X.H. Han, G.Z. Wang, J.S. Jie, X.L. Zhu, and J.G. Hou, *Thin Solid Films* **491**, 249 (2005).
- [10] Y.M. Kim, M. Yoon, I.-W. Park, Y.J. Park, and J.H. Lyou, *Sol. St. Commun.* **129**, 175 (2004).
- [11] J.H. Park, M.G. Kim, H.M. Jang, S. Ryu, and Y.M. Kim, *Appl. Phys. Lett.* **84**, 1338 (2004); E.C. Lee and K.J. Chang, *Phys. Rev. B* **69**, 085205 (2004); N.A. Spaldin, *Phys. Rev. B* **69**, 125201 (2004).
- [12] H.S. Hsu, J.C.A. Huang, Y.H. Huang, Y.F. Liao, M.Z. Lin, C.H. Lee, J.F. Lee, S.F. Chen, L.Y. Lai, and C.P. Liu, *Appl. Phys. Lett.* **88**, 242507 (2006).
- [13] C. Huang, Y. Guo, X. Liu and Y. Wang, *Thin Solid Films* **505**, 141 (2006).
- [14] G.J. Huang, J.B. Wang, X.L. Zhong, G.C. Zhou, and H.L. Yan, *J. Mater. Sci.* **42**, 6464 (2007).
- [15] X.F. Wang, J.B. Xu, N. Ke, J.G. Yu, J. Wang, Q. Li, H.C. Ong, and R. Zhang, *Appl. Phys. Lett.* **88**, 223108 (2006).
- [16] W.B. Jian, Z.Y. Wu, R.T. Huang, F.R. Chen, J.J. Kai, C.Y. Wu, S.J. Chiang, M.D. Lan, and J.J. Lin, *Phys. Rev. B* **73**, 233308 (2006).
- [17] J.M.D. Coey, M. Venkatesan and C.B. Fitzgerald, *Nat. Mater.* **4**, 173 (2005); P.I. Archer, P.V. Radovanovic, S.M. Heald, and D.R. Gamelin, *J. Am. Chem. Soc.* **127**, 14479 (2005).
- [18] D.P. Norton, M. Ivill, Y. Li, Y.W. Kwon, J.M. Erie, H.S. Kim, K. Ip, S.J. Pearton, Y.W. Heo, S. Kim, B.S. Kang, F. Ren, A.F. Hebard, and J. Kelly, *Thin Solid Films* **496**, 160 (2006).
- [19] K.R. Kittilstved, D.A. Schwartz, A.C. Tuan, S.M. Heald, S.A. Chambers, and D.R. Gamelin, *Phys. Rev. Lett.* **97**, 037203 (2006).
- [20] H. Liu, X. Zhang, L. Li, Y.X. Wang, K.H. Gao, Z.Q. Li, R.K. Zheng, S.P. Ringer, B. Zhang, and X.X. Zhang, *Appl. Phys. Lett.* **91**, 072511 (2007).
- [21] Z.M. Tian, S.L. Yuan, S.Y. Yin, S.Q. Zhang, H.Y. Xie, J.H. Miao, Y.Q. Wang, J.H. He, and J.Q. Li, *J. Magn. Magn. Mater.* **320**, L5 (2008).
- [22] D. Iuşan, B. Sanyal, and O. Eriksson, *J. Appl. Phys.* **101**, 09H101 (2007).
- [23] L. Vegard, *Z. Phys.* **5**, 17 (1921).
- [24] D. Mardare, V. Nica, C.M. Teodorescu, and D. Macovei, *Surf. Science* **601**, 4479 (2007).
- [25] B.K. Teo, *EXAFS: Basic Principles and Data Analysis*, Springer, Berlin (1983).

- [26] J. Dicarolo and A. Navrotsky, *J. Am. Ceram. Soc.* **76**, 2465 (1993).
- [27] R. Grimes and A. Fitch, *J. Mater. Chem.* **1**, 461 (1991).
- [28] C.M. Teodorescu, J.M. Esteva, M. Womes, A. El Afif, R.C. Karnatak, A.M. Flank, and P. Lagarde, *J. El. Spectrosc. Relat. Phenom.* **106** (2000) 233.
- [29] C.G. Shull, W.A. Strauser and E.O. Wollan, *Phys. Rev.* **83**, 333 (1951).
- [30] A. Kirilyuk, K. Demyk, G. von Helled, G. Meijer, A.I. Poteryaev, A.I. Lichtenstein, *J. Appl. Phys.* **93**, 7379 (2003).
- [31] H. Beinert, R.H. Holm and E. Munck, *Science* **277** (1997); T.L. Chasse and C.B. Gorman, *Langmuir* **20**, 8792 (2004); P. Hinchliffe and L.A. Sazanov, *Science* **309**, 771 (2005).
- [32] G.E. Johnson, J.U. Reveles, N.M. Reilly, E.C. Tyo, S.N. Khanna, and A.W. Castleman, *J. Phys. Chem. A* **112**, 11330 (2008); F. Xiao and H. Frei, *Angew. Chem. Intl. Ed.* **48**, 1841 (2009).
- [33] Q.S. Yin, J.M. Tan, C. Besson, Y.V. Geletii, D.G. Musaev, A.E. Kuznetsov, Z. Luo, K.I. Hardcastle, and C.L. Hill, *Science* **328**, 5976 (2010).